# Orientational phase diagram of the epitaxially strained Si(001): Evidence of a singular (105) face

L. Persichetti, A. Sgarlata, G. Mattoni, M. Fanfoni, and A. Balzarotti
*Dipartimento di Fisica, Università di Roma Tor Vergata, Via della Ricerca Scientifica, 1-00133 Roma, Italy*
(Received 17 February 2012; revised manuscript received 20 April 2012; published 11 May 2012)

By exploiting the misfit strain of Ge on Si epitaxy, we examine the significant changes induced by surface stress in the polar structural phase diagram of Si(001) surfaces. Under compressive strain, the atomic and mesoscale structures of the vicinal Si(001) surfaces are converted into a new singular (105) face which does not exist on the strain-free equilibrium shape of Si and Ge. The observed structural modifications of substrates have far-reaching implications for the Stranski-Krastanov evolutionary path of three-dimensional islanding.

DOI: 10.1103/PhysRevB.85.195314 PACS number(s): 68.35.bg, 68.37.Ef, 62.23.Eg

## I. INTRODUCTION

Being at the basis of a large portion of the properties of surfaces and interfaces, the determination of atomic surface structure is a major issue facing modern nanoscience. Surface reconstruction at the atomic length scale, in turn, determines the structural features of steps and terraces and thus the surface morphology at the mesoscale. From a thermodynamic standpoint, the bridge between these two length scales is the surface free energy $\gamma(\hat{n})$ which captures the energetics of atomic relaxation/reconstruction and of step formation as a function of the crystallographic orientation. The diagram giving the orientational dependence of surface energy is known as the $\gamma$ plot and offers a convenient way to assess the relative stability of different surface structures. In the polar plot, cuspidal points correspond to singular orientations and connecting branches to staircaselike vicinal surfaces made of terraces of the closest low-index orientation alternated with atomic steps. The determination of the equilibrium structure of clean crystalline surfaces is a classic problem of surface science[1] and comprehensive studies addressing this issue are available.[2,3] During the last decade, however, there has been an increasing need to understand how the surface structure is modified by a source of external strain, such as adsorption or heteroepitaxial growth. This requires taking into account the strain-induced changes of the $\gamma$ plot, about which little is known. In this paper, we show that surface strain causes radical modifications of the polar plot of the surface energy for the paradigmatic (001) surface of silicon.[4] By exploiting the epitaxial strain of Ge/Si growth, we explore the equilibrium shape and structure of Si for crystal orientations vicinal to the singular (001) surface through a detailed scanning tunneling microscopy (STM) investigation. For a small-miscut surface along an azimuth 45° away from the [110] direction and polar angle $\theta$ toward the [100] direction, we find that $(2 \times 1)$ symmetry is broken in the presence of misfit strain and that, as a result, nominal vicinal (001) surfaces transform into vicinal surfaces of a *new* singular {105} face which does not exist on the strain-free equilibrium shape of Si and Ge surfaces. We demonstrate that the critical polar angle of this structural transition as well as the appearance of a {105} cusp in the surface energy diagram of strained Si can be predicted by incorporating atomistic values of surface energy into a mesoscale statistical mechanical description of the step free energy. In addition, we show that the strain-induced changes in the polar phase diagram of Si provide the underlying explanation for the long-standing issue of stability of {105}-faceted three-dimensional (3D) islands observed in Ge/Si(001) heteroepitaxy.[5–7]

## II. EXPERIMENT

Experiments were carried out in an ultrahigh vacuum chamber operating at a base pressure of $p < 3 \times 10^{-11}$ Torr. The intrinsic and the strained structures of Si surfaces with crystallographic orientations finitely removed from the singular (001) face were systematically imaged using negative sample bias ~2 V and tunneling current ~200 pA by high-resolution STM. The substrates were cleaned *in situ* by a flashing procedure at 1473 K (Ref. 8) and thermally equilibrated at 873 K for several minutes. Epitaxially strained Si surfaces were obtained by the pseudomorphic growth of Ge at 873 K at constant flux of $3 \times 10^{-4}$ ML/s [1 monolayer (ML) corresponds to $6.3 \times 10^{14}$atoms/cm$^2$]. In particular, the region of the $\gamma$ plot ranging between $\theta = 6^\circ$ and $\theta = 12.5^\circ$, i.e., Si(001) vicinal substrates misoriented toward the [100] direction, revealed the most striking structural changes and are discussed here. Also Si(001) vicinals misoriented toward the [110] direction were measured for comparison. The uncertainty on the offcut angle was $\pm 0.5^\circ$.

## III. RESULTS AND DISCUSSION

### A. Strain and angular dependence of the wetting-layer morphology

Figure 1 shows the effect of increasing amounts of Ge on the Si surface morphology as a function of the misorientation angle $\theta$ counted from the (001) face. The left-end STM images show the strain-free arrangement of these surfaces. On the 6.0°-miscut surface [Fig. 1(a)], the $(2 \times 1)$ reconstruction of the singular Si(001) surface is preserved, but the long-range periodicity is broken by the faceting of steps into a dense array of kinks shown by the 3D image of Fig. 2(a). Since ⟨010⟩ steps are energetically very unfavorable,[9] kinks are introduced to compensate for the misorientation along [100]. Thus, the average ⟨010⟩ step profile consists of alternating [110] and [$\bar{1}$10] step segments and forming a 45° angle with the $(2 \times 1)$ dimer rows, as schematically depicted in Fig. 2(d). By slightly increasing the miscut angle to 6.5° [Fig. 1(d)], a nanoscale ridge pattern, due to the faceting of $(2 \times 1)$ terraces along the two perpendicular ⟨110⟩ directions,

 

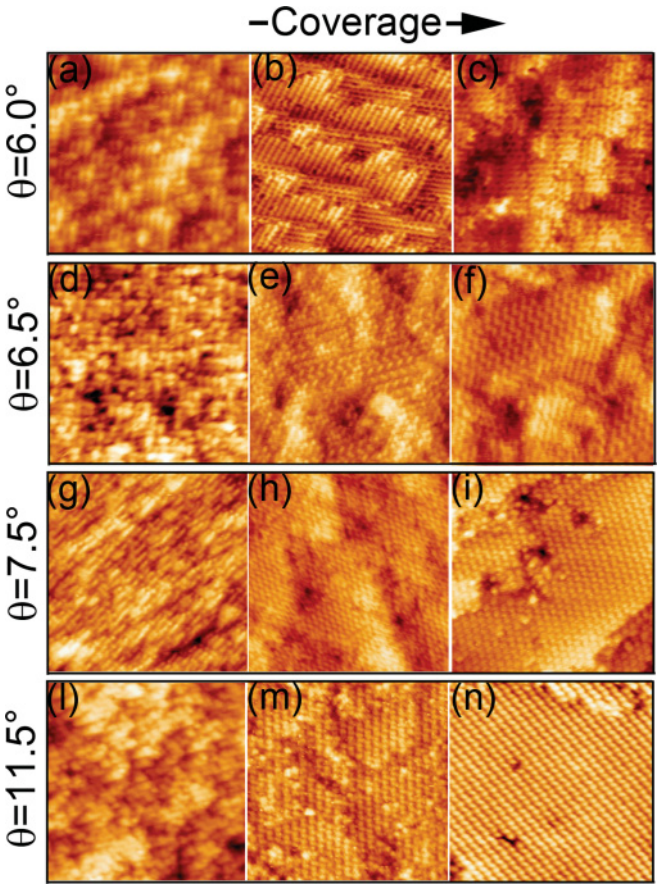


FIG. 1. (Color online) STM images, (24 × 24) nm$^2$, showing the strain-induced structural evolution of vicinal Si(001) surfaces at increasing Ge coverage: (a, d, g, l) clean surfaces; (b, e, h, m) 0.4 ML of Ge; (c, f, i, n) 1.3 ML of Ge. Image (n) was taken with positive sample bias. The effect of voltage reversal on surface reconstruction imaging is that expected from the RS model. $\theta$ is the misorientation angle from the (001) face toward the [100] direction. In the images, the horizontal and vertical axes are oriented along the ⟨110⟩ directions.

is still discernible, though the average width of terraces is roughly 2 nm and thus comparable to the dimension of the (2 × 1) unit cell. A further misorientation destroys the (2 × 1) reconstruction, resulting, for $\theta \geqslant 7.5^\circ$ [Figs. 1(g) and 1(l)], in a rugged surface (root-mean square roughness $\sigma \simeq 1$ Å) without an ordered mesoscale structure. The disappearance of the usual stepped morphology of the vicinal (001) surface is due to the subtle interplay between the atomic and mesoscale topologies of the surface. If one considers the smallest (2 × 1)-reconstructed terrace which satisfies the constraint of a mean ⟨010⟩ orientation of steps, it is easy to see that it should consist of at least four unit cells stacked along the [110] direction in order to avoid step crossing [see inset of Fig. 2(c)]. Thus, the nanoscale structure sets a limit, $L_c$, for the average terrace width of stable (001) surfaces which corresponds to $\theta \simeq 7.5^\circ$ [Fig. 2(c)]; this matches well with the experimental results. We stress that this constraint is not present along the [110] direction and, consequently, stable (001) vicinal surfaces are observed up to $\theta > 10^\circ$.[3,7] The atomic structure has a major impact on the global surface morphology under epitaxial strain, as is shown in the following paragraph.

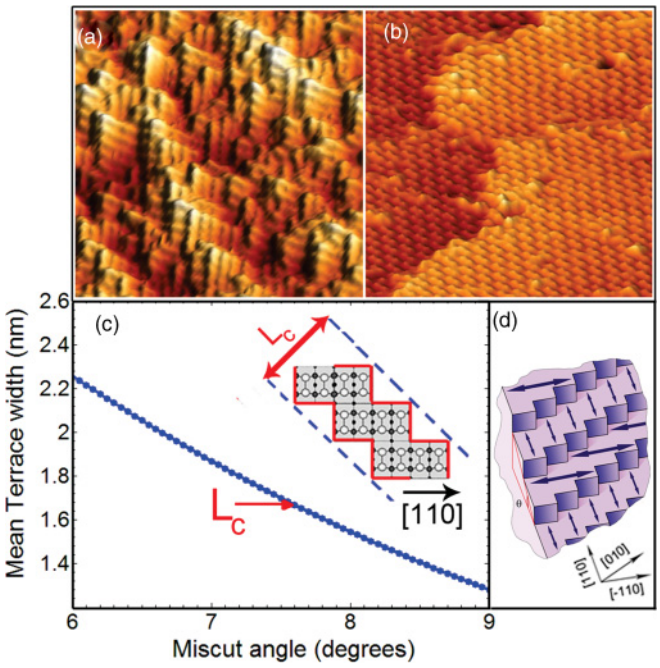


FIG. 2. (Color online) (a) STM image, (25 × 25) nm$^2$, showing the kinked structure and the (2 × 1) reconstruction of the 6°-miscut Si(001) surface. (b) STM image, (36 × 36) nm$^2$ , showing the step structure and the RS reconstruction of the singular (105) surface. (c) Geometrical dependence of the average terrace width for a mixture of single- and double-height steps (Ref. 23). In the inset, the smallest (2 × 1)-reconstructed terrace with a mean ⟨010⟩ step orientation is shown. $L_c$ is the corresponding average terrace width. (d) Schematic drawing of a vicinal Si(001) surface misoriented toward the [100] direction. Double arrows indicate the alternating (1 × 2)-(2 × 1) structure of adjacent terraces.

During the two-dimensional (2D) early stages of Ge/Si epitaxy, the growing overlayer is pseudomorphically compressed by the lattice misfit strain $\varepsilon_m = -4.3\%$ between Ge and Si. On the 6°-miscut surface, the misfit strain promotes local modifications in the (2 × 1) reconstruction, such as formation of $c(4 \times 2)$-reconstructed patches [Fig. 1(b)] and arrays of dimer vacancies [Fig. 1(c)], which reduce partially the surface lattice deformation. This evolution differs slightly from that observed on the singular (001) surface[5,6,10] and does not alter the overall surface texture. This is no longer the case for the initially rough surfaces, shown in Figs. 1(g) and 1(l), which undergo extended structural changes with Ge deposition. On these surfaces, the misfit strain leads to a progressive ordering during which $\sigma$ is reduced by a factor of ∼10. At the atomic scale, such a rearrangement is driven by the rebonded-step (RS) reconstruction [Figs. 1(h) and 1(m)] which usually covers the {105} facets of 3D Ge islands in Si(001) epitaxy. Such a surface reorganization is not restricted to the atomic reconstruction but involves the buildup of the terrace-step morphology characteristic of a vicinal surface [Figs. 1(i) and 1(n)]. The question is the following: Which singular face are the surfaces just described vicinal to? In previous seminal works,[11–13] even though the RS reconstruction was observed on the Si(105) crystal surface ($\theta = 11.3^\circ$) after Ge deposition, the structure of the surface was interpreted as that of a Si(001) vicinal composed by a staircase of (001) nanofacets. However,

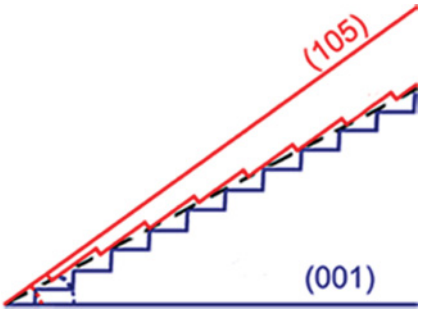


FIG. 3. (Color online) The alternative step structures of a vicinal (001) and (105) surface.

this is not consistent with our high-resolution STM images showing atomically flat terraces ($\sigma \simeq 0.1$ Å) separated by monoatomic steps [Figs. 1(n) and 2(b)]. Indeed, the flatness of the strained (105) surface[14] is comparable with that of a singular orientation. Furthermore, our findings reveal that, starting from a critical polar angle $\theta_c = 6.5^\circ$, strained Si surfaces form a family of surfaces vicinal to this new singular face [Figs. 1(f) and 1(i)]. As schematically sketched in Fig. 3, these surfaces have terraces which are parallel to the (105) face rather than to the (001) plane. Thus a nominal polar angle of, e.g., $\theta = 10.5^\circ$ is only $\sim 1^\circ$ off the (105) plane and, hence, the corresponding terrace widths are much larger than those at the same miscut angle toward the [110] direction, for which terraces are (001) oriented (Fig. 4). We emphasize that the emergence of (105) vicinals is not merely due to the geometrical constraint which hampers $(2 \times 1)$-reconstructed surfaces at high polar angles. This is clearly apparent from the structural transformation occurring at $\theta = \theta_c$ [Figs. 1(d) to 1(f)]. By increasing Ge coverage, the initial $(2 \times 1)$ reconstruction converts progressively to the RS reconstruction, as evidenced by the 45° rotation from the ⟨110⟩ orientation of the $(2 \times 1)$ dimers to the ⟨100⟩ orientation of the RS rows [Fig. 1(e)]. Ultimately, the overall surface structure is changed since small and highly kinked (001) terraces are replaced by much larger and regular (105) terraces [Fig. 1(f)]. This indicates that the (001)-to-(105) phase transition is not just a matter of geometry, but is also driven by an effective energy gain.

The surface energy $\gamma(\hat{n})$ of a vicinal surface is usually expanded as $\frac{\gamma(\hat{n})}{\cos\theta} = \gamma(\hat{n}_0) + \frac{\chi(d)}{d}$, where $\gamma(\hat{n}_0)$ is the free energy of the singular face itself and $\chi(d) = \beta + g(d)$ is the free energy per unit length of a step on the vicinal surface. The latter term includes the energy $\beta$ of an isolated step and the interaction energy $g(d)$ between steps having average distance $d = h/\tan(\theta)$ and step height $h$. Since steps interact essentially as linear elastic dipoles,[15,16] such interaction energy is $g(d) = A/d^2$. As illustrated in Fig. 3, a vicinal orientation $n$ intermediate between the (001) and the (105) planes can, in principle, be built with either (001) or (105) terraces[17] and the surface energy of these two structures is obtained from the expansion of $\gamma(\hat{n})$ around $\theta_{001} = 0^\circ$ or $\theta_{105} = 11.3^\circ$, respectively:

$$\gamma_i(\hat{n}) = \gamma_i \cos(\theta_i - \theta) + \frac{\beta_i}{h_i} |\sin(\theta_i - \theta)| + \frac{A}{h_i^3} \frac{|\sin^3(\theta_i - \theta)|}{\cos^2(\theta_i - \theta)}, \quad (1)$$

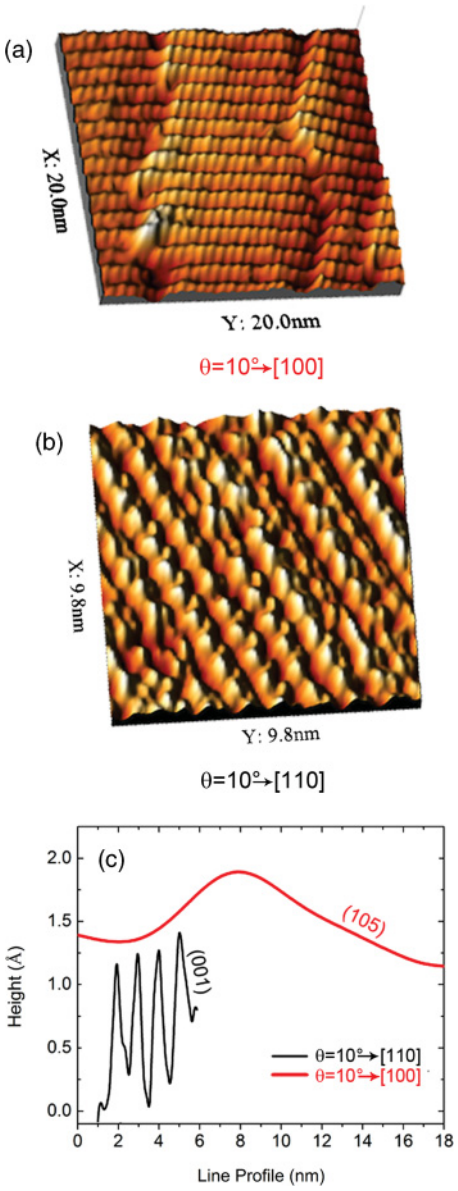


FIG. 4. (Color online) STM images of a vicinal (105) surface [panel (a)] and a vicinal (001) surface [panel (b)] at a polar angle of $\theta = 10^\circ$ and azimuthal misorientation toward the [110] and the [100] directions, respectively. The vicinal (105) surface has markedly larger terraces, as evident from the corresponding line profiles shown in panel (c).

where $i \in \{(001),(105)\}$ is the reference direction. The $\gamma$ plot gives, by definition, the most energetically favored structure at each polar angle and, therefore, corresponds to the lower envelope of the previous functions. Since our goal is to obtain the polar energy diagram of epitaxially strained surfaces, we set $\gamma_{001} = 60.5$ meV/Å$^2$ and $\gamma_{105} = 58.7$ meV/Å$^2$, which correspond, respectively, to the *ab initio* surface energies[14,18] of Ge(001) and Ge(105) compressively strained to the Si lattice constant ($\varepsilon_m = -4.3\%$). The free energy per unit length of faceted (001) steps ($h_{001} = 1.36$ Å)[19] and the free energy per unit length of faceted (105) steps ($h_{105} = 0.55$ Å) are $\beta_{001} = 18.3$ meV/Å[9] and $\beta_{105} = 12$ meV/Å.[20] Since the relevant energy scale of the step interaction strength $A$ is

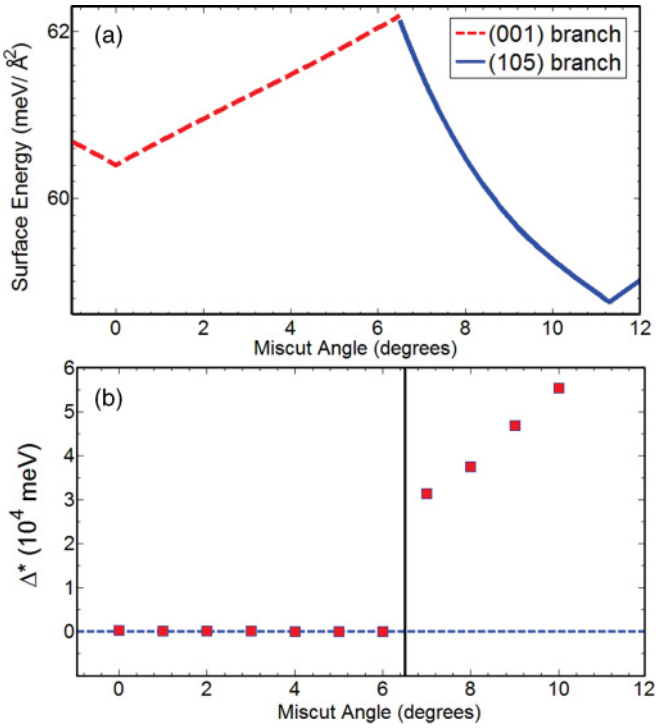


FIG. 5. (Color online) (a) Experimental $\gamma$ plot of strained Si between the (001) and the (105) orientations. (b) Activation energy for {105} islanding as a function of the miscut polar angle.

mainly determined by the properties of bulk Si crystal,[21] the small polar dependence of $A$ for vicinal Si surfaces of different orientations can be neglected and an average value of ~500 meV/Å (Ref. 22) in the angular range between the (001) and the (111) faces ($\theta = 0^\circ$ to $54.7^\circ$)[23,24] can be taken.

Despite these approximations, the resulting $\gamma$ plot, shown in Fig. 5(a), captures the essential features of our experimental findings, namely, the appearance of two cusps in the correspondence of the (001) and the (105) orientations. The latter acts as a singular face in the presence of epitaxial strain. Furthermore, also the competition between (001) and (105) vicinals, experimentally observed at intermediate polar angles, is closely reproduced. Once a source of external strain is introduced through Ge deposition, i.e., the crystal surface is stretched to the mismatch strain $\varepsilon_m$, the (001) vicinal structure remains energetically favored for $\theta \leqslant 6^\circ$. This is exactly what it is inferred from the STM images reported here for $\theta = 6^\circ$ (Fig. 1) and in previous studies for $\theta < 5^\circ$.[25,26] For $\theta$ values larger than $6^\circ$, the (105) vicinal structure is more stable and, thus, it is formed under Ge deposition. Depending on the structure of the strain-free substrate, two different pathways exist: (i) the (105) atomic texture replaces the preexisting $(2 \times 1)$ reconstruction of the (001) terrace at $6.5^\circ$, and (ii) the (105) structure evolves from the initially rough surface at higher miscut angles for which the $(2 \times 1)$ reconstruction is geometrically hindered. In line with the symmetric shape of the (105) branch of the $\gamma$ plot around the (105) cusp, Fig. 6 shows that the structural evolution on a Si surface with a misorientation of $12.5^\circ$ along the [100] direction is the same as that observed at polar angles slightly lower than the (105) singular face: The initially rough morphology of the clean

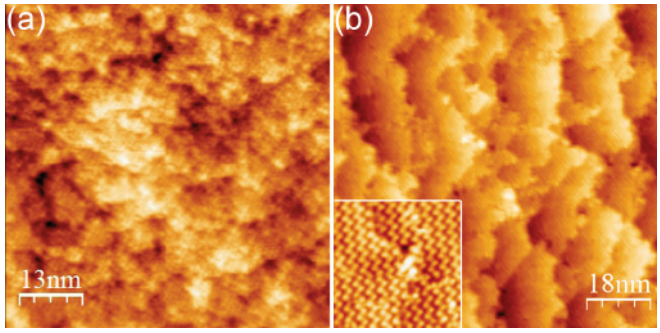


FIG. 6. (Color online) Structural evolution induced by Ge deposition of a $12.5^\circ$-miscut Si(001) along the [100] direction: (a) rough morphology of the clean surface; (b) stepped morphology at a Ge coverage of 1.5 ML. The terraces show the RS reconstruction of the (105) face, as indicated by the STM image, $(14 \times 14)$ nm$^2$, reported in the inset.

surface [Fig. 6(a)] is converted by Ge deposition into a vicinal (105) stepped morphology [Fig. 6(b)].

### B. Effect of the wetting-layer structure on 3D islanding

The structural symmetry of the substrate is probably the crucial parameter determining the shape and stability of epitaxially grown 3D nanostructures. In fact, it is well known that Ge islands grown on flat[27,28] and vicinal[29,30] Si(001) surfaces show a bimodal behavior with shallow {105}-faceted islands ("pyramids") at small volumes and larger islands ("domes") with facets of steeper orientations. Underlying this growth behavior is the relevant surface energy gain of the {105} facets with respect to the (001) wetting layer (WL), the key feature providing the thermodynamic stability of pyramids.[31] Indeed, even though the elastic strain relaxation of shallow pyramids is rather limited compared with domes, the lowering in surface energy associated with {105} faceting makes the formation of pyramids basically a nonactivated process[32,33] clearly favorable at the early stages of growth.

To be quantitative, consider the free-energy difference $\Delta$ between a 3D pyramid and a 2D WL of the same volume $V$, which is

$$\Delta = (\rho_{pyr} - \rho_{WL})V + (\alpha_{105}C_S - \gamma_{WL}C_B)V^{2/3}. \qquad (2)$$

Here, $\rho_{pyr}$ and $\rho_{WL}$ are the elastic-energy density stored, respectively, in the island (including substrate deformation) and in the WL; $\alpha_{105}$ is the average surface energy of the {105} island facets; $\gamma_{WL}$ is the surface energy of the WL; and $C_S = S/V^{2/3}$ and $C_B = B/V^{2/3}$ are shape-dependent coefficients which quantify the relative weight of the facet area $S$ and the WL area $B$ covered by the island. The resulting activation barrier for the formation of pyramids is $\Delta^* = 4(\alpha_{105}C_S - \gamma_{WL}C_B)^3/27(\rho_{pyr} - \rho_{WL})^2$. In order to estimate the barrier height as a function of polar angle, we exploited continuum elasticity theory and finite element solutions to model strain energy relaxation using strain-dependent corrections to *ab initio* calculated surface energies[14] for {105} facets of Ge pyramids over the entire range of substrate orientations. Aiming to emphasize the stability of {105} islands in relation to the miscut-dependent structure of low-index terraces, we set $\gamma_{WL} = \gamma_{001}$ for $\theta < \theta_c$, for which terraces

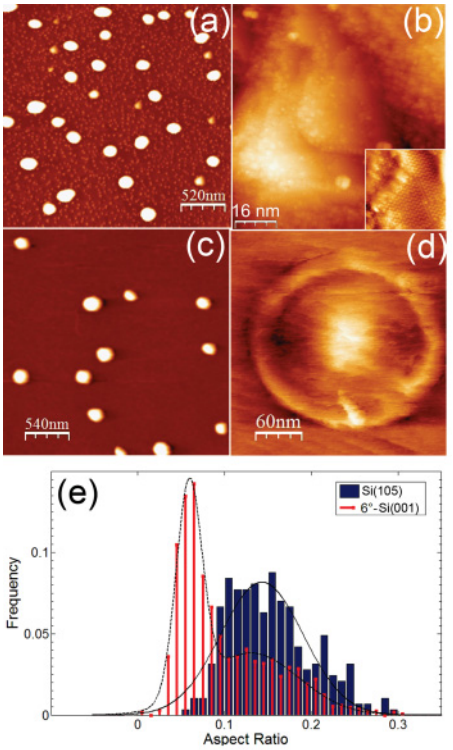


FIG. 7. (Color online) (a, b) STM images of the 6°-miscut Si(001) surface. (a) Bimodal island distribution at a coverage of 5.5 ML of Ge. (b) Snapshot of a skewed pyramid bounded by {105} facets. In the inset, (20 × 20) nm$^2$, the RS reconstruction of the facets is evident. (c, d) STM images of the 7.5°-miscut Si(001) surface. (c) Unimodal distribution of domes at a coverage of 5.5 ML of Ge. (d) Precursor of domes growing from the planar WL. (e) Distribution of the island aspect ratio on a 6°-miscut Si(001) surface and a Si(105) surface. The two distributions are fitted to Gaussian functions.

maintain the orientation of the (001) singular surface, and $\gamma_{WL} = \gamma_{105}$ at higher polar angles at which terraces are parallel to the (105) face. As expected, we find that the nucleation of {105} islands on (001) terraces does not require overcoming a barrier, whereas the nucleation on the {105} terraces is an activated process with finite activation barriers [Fig. 5(b)]. Intuitively, the surface energy gain of {105} pyramids over the WL is counterbalanced by the formation of a highly stable RS-reconstructed wetting layer. Being energetically activated, nucleation of pyramids requires large fluctuations to form clusters of critical size; therefore it is definitely not a plausible kinetic route at low Ge coverage compared to the thickening of a low-surface-energy 2D film. At larger coverage, instead, the system is prone to choose the steeper dome shape to relieve strain more efficiently.

Indeed, experimental results indicate that, until the (001) structure of the substrate is preserved, the usual evolutionary path of Ge/Si epitaxy is followed: {105} islands formed at earliest stages of growth coexist with domes at larger coverage [Figs. 7(a)]. Due to the misorientation from the (001) plane, {105} pyramids have however truncated skewed shapes [Fig. 7(b)].[26] A statistical analysis of the island's aspect ratio (height versus square root of the island's base area) clearly shows a bimodal shape distribution which is nicely fitted to a double-peak Gaussian function [Fig. 7(e)].

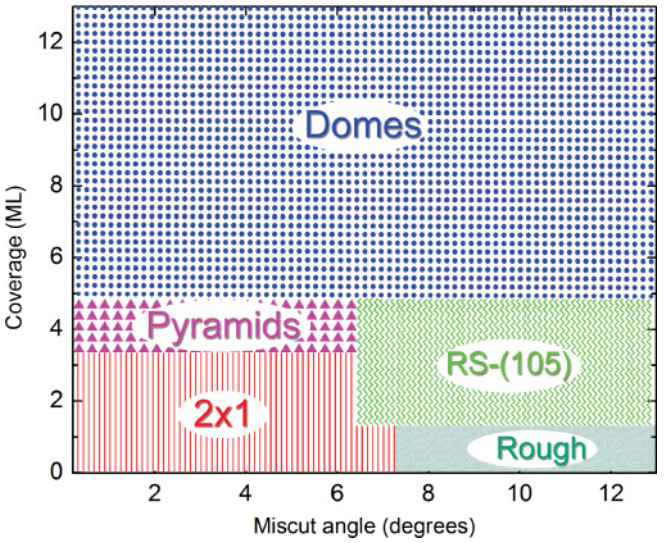


FIG. 8. (Color online) Schematic orientational phase diagram of Si surfaces vicinal to the (001) and the (105) planes along the [100] direction, as a function of Ge coverage. The sharp boundaries are for guidance only.

The emergence of a strain-induced branch in the $\gamma$ plot of the substrate, favoring the flat RS-reconstructed WL against pyramid nucleation, delays the onset of 3D islanding to larger critical coverage (about 5 ML instead of 3.5 ML) above which only domes are observed [Figs. 7(c)]. Indeed, the distribution of aspect ratios is unimodal and shows only the single peak corresponding to domes [Fig. 7(e)]. Also the pathway leading to dome formation is changed: Domes, which usually develop from increasingly steeper pyramid facets, here evolve from seeds nucleated directly onto the planar WL [Fig. 7(d)]. This shows that the structural changes induced by epitaxial strain on vicinal surfaces result in relevant alterations of the thermodynamics of the Stranski-Krastanov growth, leading to the equilibrium phase diagram displayed in Fig. 8. The diagram schematically describes the dependence of Si surface morphology on both polar angle and Ge coverage, summarizing the results presented above. The most striking feature induced by epitaxial strain is the appearence of the RS (105) reconstruction for polar angles $\theta > 6°$: for a narrow polar range $6° < \theta < 7.5°$, a progressive transition from the (2 × 1) to the RS reconstruction is observed; for larger miscut angles for which the (2 × 1) reconstruction is geometrically hindered, the RS structure is formed from an initially rough surface. The changes in the surface structure of the substrates dramatically affect the shape and stability of islands formed during the Stranski-Krastanov Ge/Si growth. In this context, it is argued that the 3D {105} islanding is an alternative route when the formation of a planar (105) surface is hampered by energetic or geometric constraints, providing an ultimate explanation for the long-standing question of whether {105} faceting has a unique way in Ge/Si epitaxy.

## IV. CONCLUSIONS

In conclusion, experimental evidence and theoretical modeling have shown that epitaxial strain affects not only atomic reconstruction but also the whole mesoscale architecture of

surfaces. In other words, owing to the strain, a surface, which under normal conditions is left out from the polar energy diagram of stable crystal orientations, becomes strongly singular. Finally, we emphasize that our analysis may be of importance for a future scaling to lower-dimensional crystals, such as SiGe nanowires, for which the determination of the nanowire facets is a crucial issue.


## ACKNOWLEDGMENTS

We acknowledge G. Fanfoni for his assistance in the graphic design work. This work has been supported by the Queensland Government through the NIRAP project "Solar Powered Nanosensors."



[1] I. Markov, *Crystal Growth for Beginners* (World Scientific, Singapore, 2003).

[2] J. M. Bermond, J. J. Métois, X. Egéa, and F. Floret, Surf. Sci. **330**, 48 (1995).

[3] A. A. Baski, S. C. Erwin, and L. J. Whitman, Surf. Sci. **392**, 69 (1997).

[4] A. Sgarlata, L. Persichetti, and A. Balzarotti, in *Surface and Interface Science*, edited by K. Wandelt (Wiley-VCH, Weinheim, 2012), in press.

[5] J. Stangl, V. Holý, and G. Bauer, Rev. Mod. Phys. **76**, 725 (2004).

[6] B. Voigtländer, Surf. Sci. Rep. **43**, 127 (2001).

[7] I. Berbezier and A. Ronda, Surf. Sci. Rep. **64**, 47 (2009).

[8] A. Sgarlata, P. D. Szkutnik, A. Balzarotti, N. Motta, and F. Rosei, Appl. Phys. Lett. **83**, 4002 (2003).

[9] H. J. W. Zandvliet, O. Gurlu, R. van Gastel, and B. Poelsema, Phys. Rev. B **69**, 125311 (2004).

[10] L. V. Arapkina and V. A. Yuryev, J. Appl. Phys. **109**, 104319 (2011).

[11] M. Tomitori, K. Watanabe, M. Kobayashi, F. Iwawaki, and O. Nishikawa, Surf. Sci. **301**, 214 (1994).

[12] Y. Fujikawa, K. Akiyama, T. Nagao, T. Sakurai, M. G. Lagally, T. Hashimoto, Y. Morikawa, and K. Terakura, Phys. Rev. Lett. **88**, 176101 (2002).

[13] T. Eguchi, Y. Fujikawa, K. Akiyama, T. An, M. Ono, T. Hashimoto, Y. Morikawa, K. Terakura, T. Sakurai, M. G. Lagally, and Y. Hasegawa, Phys. Rev. Lett. **93**, 266102 (2004).

[14] D. B. Migas, S. Cereda, F. Montalenti, and L. Miglio, Surf. Sci. **556**, 121 (2004).

[15] V. I. Marchenko and A. Y. Parshin, Sov. J. Exp. Theor. Phys. **52**, 129 (1980).

[16] H.-C. Jeong and E. D. Williams, Surf. Sci. Rep. **34**, 171 (1999).

[17] Subject to the geometrical constraint discussed heretofore.

[18] G. H. Lu, M. Cuma, and F. Liu, Phys. Rev. B **72**, 125415 (2005).

[19] Equation (1) can be straightforwardly modified to take into account the presence of double-height steps on vicinal (001) surfaces, but this does not significantly affect the resulting $\gamma$ plot.

[20] S. Cereda, F. Montalenti, and L. Miglio, Surf. Sci. **591**, 23 (2005).

[21] C. Misbah, O. P. Louis, and Y. Saito, Rev. Mod. Phys. **82**, 981 (2010).

[22] Variations of the value of $A$, however, do not alter substantially our findings.

[23] L. Persichetti, A. Sgarlata, M. Fanfoni, M. Bernardi, and A. Balzarotti, Phys. Rev. B **80**, 075315 (2009).

[24] G. Prévot, F. Leroy, B. Croset, Y. Garreau, A. Coati, and P. Müller, Surf. Sci. **606**, 209 (2012).

[25] P. Sutter, E. Sutter, and L. Vescan, Appl. Phys. Lett. **87**, 161916 (2005).

[26] B. J. Spencer and J. Tersoff, Appl. Phys. Lett. **96**, 073114 (2010).

[27] G. Medeiros-Ribeiro, A. M. Bratkovski, T. I. Kamins, D. A. A. Ohlberg, and R. S. Williams, Science **279**, 353 (1998).

[28] F. M. Ross, R. M. Tromp, and M. C. Reuter, Science **286**, 1931 (1999).

[29] L. Persichetti, A. Sgarlata, M. Fanfoni, and A. Balzarotti, Phys. Rev. Lett. **104**, 036104 (2010).

[30] L. Persichetti, A. Capasso, A. Sgarlata, M. Fanfoni, N. Motta, and A. Balzarotti, in *Self-Assembly of Nanostructures*, edited by S. Bellucci (Springer, New York, 2012), Vol. 12 of Lecture Notes in Nanoscale Science and Technology, Chap. 4, pp. 201–263.

[31] P. Raiteri, D. B. Migas, L. Miglio, A. Rastelli, and H. von Känel, Phys. Rev. Lett. **88**, 256103 (2002).

[32] R. M. Tromp, F. M. Ross, and M. C. Reuter, Phys. Rev. Lett. **84**, 4641 (2000).

[33] P. Sutter and M. G. Lagally, Phys. Rev. Lett. **84**, 4637 (2000).